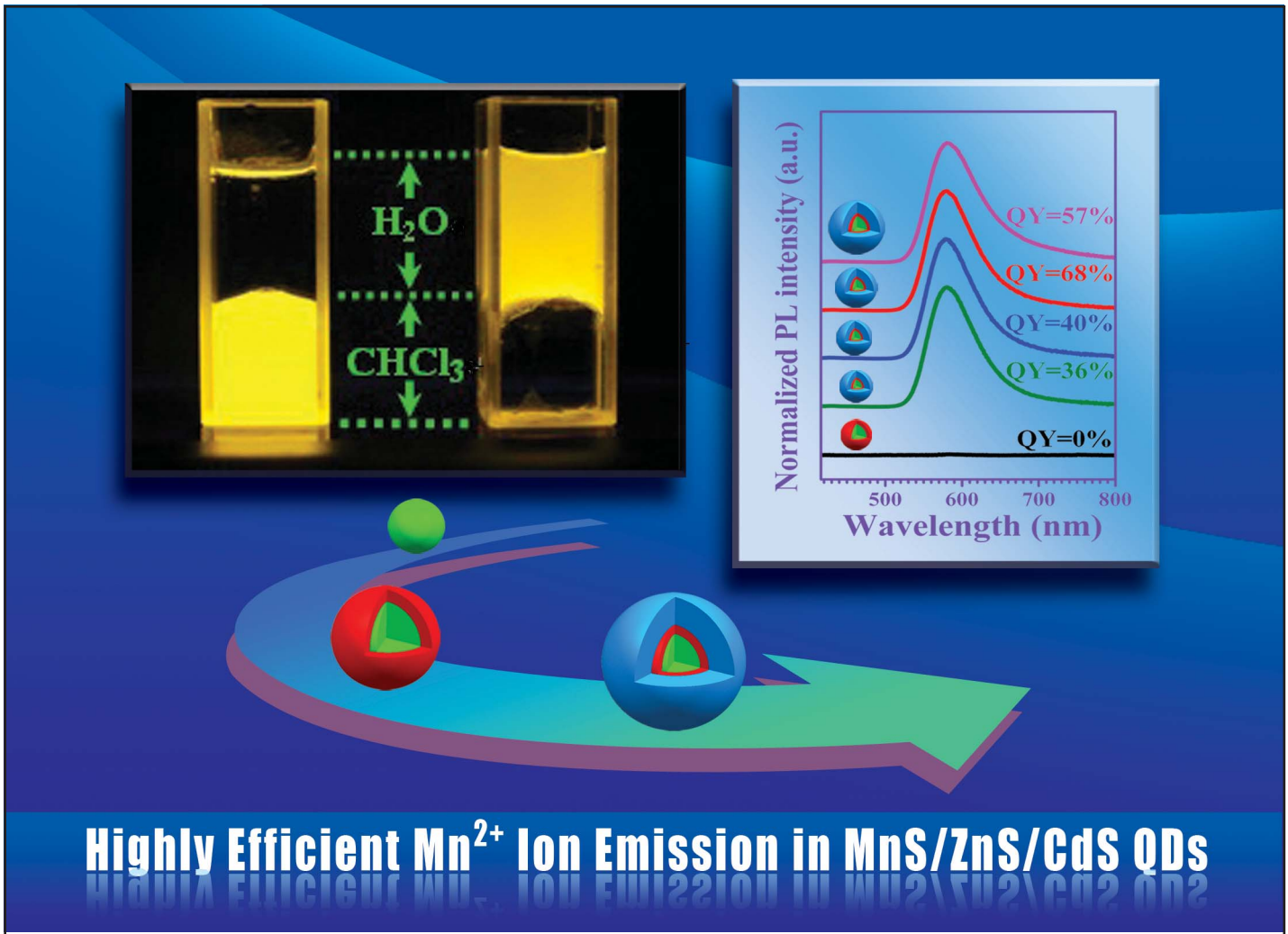

Highly Efficient Mn^{2+} Ion Emission in MnS/ZnS/CdS QDs

Nanomaterials Group of Prof. Weiyou Yang at Ningbo University of Technology commits to the controlled growth, optoelectronic properties, and device applications of semiconductor nanostructures such as SiC and transition-metal-doped quantum dots.

Title: Highly efficient and well-resolved Mn^{2+} ion emission in MnS/ZnS/CdS quantum dots

This work reports highly efficient and well-resolved Mn^{2+} ion emission in MnS/ZnS/CdS QDs with a PL QY of up to 68%. The QDs can be made water-soluble and also coated by ligands with short carbon chain lengths with almost no loss of PL QY.

As featured in:

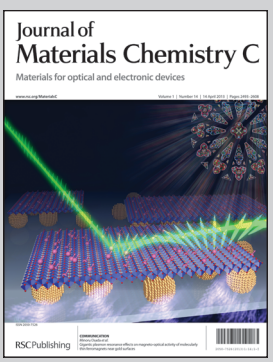

See S. Cao *et al.*,
J. Mater. Chem. C, 2013, **1**, 2540.

RSC Publishing

www.rsc.org/MaterialsC

Registered Charity Number 207890

Journal of Materials Chemistry C

RSC Publishing

PAPER

View Article Online
View Journal | View Issue

Highly efficient and well-resolved Mn^{2+} ion emission in MnS/ZnS/CdS quantum dots†

Cite this: *J. Mater. Chem. C*, 2013, **1**, 2540

Sheng Cao,‡[ab] Jinju Zheng,‡[bc] Jialong Zhao,[d] Lin Wang,[b] Fengmei Gao,[b] Guodong Wei,[b] Ruosheng Zeng,[e] Linhai Tian*[a] and Weiyou Yang*[b]

Received 5th November 2012
Accepted 18th February 2013

DOI: 10.1039/c3tc00561e

www.rsc.org/MaterialsC

We demonstrate a strategy for the growth of Mn^{2+} ion doped cadmium based II–VI semiconductor quantum dots (QDs) with a designed buffer layer of ZnS (MnS/ZnS/CdS or Mn:CdS QDs), which aims to meet the challenge of obtaining highly efficient and well-resolved Mn^{2+} ion emission. First, small, high quality MnS cores are obtained by using thiols to replace conventional alkyl amines as capping ligands. Then a buffer layer of ZnS with a tailored thickness is introduced to the QDs before the growth of CdS shells to reduce the size mismatch between the Mn^{2+} (dopant) and Cd^{2+} (host) ions. The fabricated MnS/ZnS/CdS core/shell QDs exhibit a high PL QY of up to 68%, which is the highest ever reported for any type of Mn^{2+} ion doped cadmium based II–VI semiconductor QD. The photoluminescence (PL) of the QDs consists of well-resolved Mn^{2+} ion emission without any detectable emission from the CdS band edge or surface defects. In addition, our MnS/ZnS/CdS QDs cannot only be made water-soluble, but can also be coated by ligands with short carbon chain lengths, nearly without cost to the PL QY, which could make them strong candidates for practical applications in biology/biomedicine and opto/electronic devices.

1 Introduction

Luminescent colloidal semiconductor nanocrystals (NCs) or quantum dots (QDs) have been extensively explored during the past decades due to their unique size and composition-tunable band edge photoluminescence (PL). Metal ion doped NCs, as a novel kind of luminescent material, not only retain nearly all the intrinsic advantages of QDs, but also possess additional merits such as large Stokes shifts (to avoid self-absorption/energy transfer), enhanced thermal and chemical stabilities, and long excited state lifetimes. This makes such doped QDs potentially excellent candidates for applications in biomedical diagnosis, solar cells, light-emitting diodes (LEDs), and so on.[1–3] Thus, the controlled synthesis of doped QDs with improved PL quantum yields (QYs) has received considerable attention recently.[4–12]

In one of the early investigations, Bhargava *et al.*[13] reported that Mn^{2+} ion doped ZnS QDs exhibited more efficient PL than their undoped counterparts. Since then, the use of Mn^{2+} ions as luminescence activators for improving the PL QY in II–VI semiconductor NCs has been studied extensively, including the use of Mn:ZnS,[9,14–18] Mn:CdS,[5,6,19–21] Mn:ZnSe,[7,10,22] Mn:CdSe,[23,24] and so on. However, unlike the case of Mn^{2+} ion doped zinc based II–VI semiconductor NCs (*e.g.* ZnS (ref. 9) and ZnSe (ref. 7 and 10)) with their intrinsic well-resolved and highly efficient Mn^{2+} ion emission, many reports suggest that doping Mn^{2+} in the Cd^{2+} sites of cadmium based II–VI semiconductor NCs is still a great challenge.[25,26] Moreover, Mn^{2+} ion emission is always accompanied by an obvious defect state emission.[1,6,27–29] Defect state PL often appears in the same spectral region as Mn^{2+} ion emission, resulting in a very broad emission feature without any distinctive features and making confirmation of these two contributions difficult. For example, Ishizumi *et al.* observed an obvious surface defect emission in addition to the Mn^{2+} ion emission in Mn:CdS/ZnS QDs even at a low temperature of 12 K.[27,28] Similar results were also reported by Sarma and Nag.[1] They even obtained white light emission by tuning the relative surface-state emissions of the NC host and the dopant. In 2007, Sarma's group[6] first obtained a distinct Mn^{2+} ion related emission in water soluble Mn:CdS QDs, which was well separated from the defect state emission. However, the PL had a

[a]*Research Institute of Surface Engineering, Taiyuan University of Technology, Taiyuan 030024, People's Republic of China. E-mail: tianlinhai@tyut.edu.cn*

[b]*Institute of Materials, Ningbo University of Technology, Ningbo 315016, People's Republic of China. E-mail: weiyouyang@tsinghua.org.cn; Tel: +86-574-87080966*

[c]*School of Mechanical Engineering, Ningbo University of Technology, Ningbo 315016, People's Republic of China*

[d]*State Key Laboratory of Luminescence and Applications, Changchun Institute of Optics, Fine Mechanics and Physics, Chinese Academy of Sciences, Changchun 130033, People's Republic of China*

[e]*School of Chemistry and Materials Science, Guizhou Normal University, Guiyang 550001, People's Republic of China*

† Electronic supplementary information (ESI) available: Summary of typical work on Mn^{2+} doped CdS and ZnCdS d-dots previously reported, calculation of ZnS/CdS layer thicknesses, PL quantum-yield (QY) experimental measurements, PL decay and data fitting of MnS/ZnS/CdS QDs. See DOI: 10.1039/c3tc00561e

‡ These authors contributed equally to this work.

QY of only 2%, and still included an obvious defect state emission. To the best of our knowledge, to date little work has been reported on the PL of Mn^{2+} ion doped cadmium based II–VI semiconductor NCs with Mn^{2+} ion related emission with a QY of higher than 30% (Table S1, ESI†).

In fact, besides the well-known surface defects due to the large surface-to-volume ratios in doped QDs, other defects resulting from local strain will also occur owing to the different ionic sizes of the dopant and host cations.[8] The size of the Mn^{2+} ion (0.67 Å) is close to that of the Zn^{2+} ion (0.74 Å), while it is considerably smaller than that of the Cd^{2+} ion (0.95 Å).[30] This might be the primary reason for the lower PL QYs in Mn:CdS (or Mn:CdSe) NCs compared to those in Mn:ZnS (or Mn:ZnSe) NCs.[4,25,31] Recently, Sarma's group[8] pointed out that the local strain induced by the size mismatch (resulting from the cation–anion bond length differences) between the dopant (Mn^{2+}) and the host (Cd^{2+}) cations could be limited by optimizing the composition of the host. They fabricated $Zn_xCd_{1-x}S$ NCs with a high dopant level of 7.5% Mn^{2+}, and the QY could be improved up to 25%. This implied that the PL properties of Mn^{2+} ion doped NCs could be profoundly enhanced by reducing the local strain between the dopants and hosts.

In the present work, we demonstrate the fabrication of Mn:CdS QDs *via* a nucleation-doping strategy, which aims to meet the challenge of obtaining highly efficient and well-resolved Mn^{2+} ion emission. Small MnS cores were obtained by using thiols to substitute conventional alkyl amines as capping ligands, which was necessary for the growth of Mn^{2+} ion doped ZnS QDs of high quality. To reduce the local strain derived from the lattice mismatch between MnS and CdS, an interface buffer layer (~1 monolayer (ML)) was introduced for the QD growth by using a designed structure of MnS/ZnS/CdS (also called Mn:CdS d-dots).[30] The fabricated MnS/ZnS/CdS QDs exhibited extremely high luminescence with an Mn^{2+} ion emission QY of up to 68%. The recombination processes of the PL in the Mn^{2+} ion doped QDs were investigated systematically by clarifying the effects of the thickness of the CdS shell and the ZnS buffer layer on the PL properties.

2 Experimental

2.1 Raw materials

The raw materials zinc stearate ($ZnSt_2$, ZnO 11.3–11.5%), cadmium stearate ($CdSt_2$, AR), sulfur powder (S, 99.99%), 1-dodecanethiol (DDT, 98%), 1-octadecanethiol (ODT, 97%), oleylamine (OLA, 70%), tetramethylammonium hydroxide ($TMAH\cdot 4H_2O$, 97%), manganese chloride ($MnCl_2\cdot 4H_2O$, ≥99%), benzylamine (BLA, AR) and benzoyl peroxide (BOP, CP) were commercially available from Aladdin company. 1-Octadecene (ODE, 90%), stearate acid (SA, 97%), and mercaptopropionic acid (MPA, 99%) were purchased from Adamas-beta company. All the chemicals were used directly without further purification.

2.2 Preparation of manganese stearate ($MnSt_2$)

The manganese precursor of $MnSt_2$ was prepared in a similar way to that reported in previous work.[7] In a typical process, 2.85 g of SA was dissolved in 30 mL of methanol, loaded into a 100 mL three necked flask, and heated up to 50–60 °C to obtain a clear solution in air followed by cooling to ~40 °C. Then a $TMAH\cdot 4H_2O$ solution (obtained by dissolving 1.81 g of $TMAH\cdot 4H_2O$ in 5 mL of methanol) was mixed with the SA solution. The obtained mixture was stirred for 15 min to make the reaction complete. Then 0.99 g of $MnCl_2\cdot 4H_2O$ dissolved in 5 mL of methanol was introduced into the mixture dropwise with vigorous stirring to obtain a white precipitate of $MnSt_2$ which was flocculated slowly. The resultant precipitate was washed repeatedly with hot methanol and dried under vacuum.

2.3 Preparation of stock solutions

S stock solution was prepared by taking 0.045 g of S powder and 0.2 mL of DDT or 0.24 g of ODT in 3 mL of ODE. Cadmium precursor solution was prepared using 0.70 g of $CdSt_2$ dissolved in 7 mL of ODE. Several concentrations of zinc precursor solutions were prepared for the fabrication of MnS/ZnS/CdS QDs with tailored thicknesses of the ZnS buffer layers. A typical zinc precursor solution was prepared by dissolving 0.06 g of $ZnSt_2$ and 0.6 mL of OLA in 3 mL of ODE.

2.4 Synthesis of MnS/ZnS/CdS QDs

The synthesis of MnS/ZnS/CdS QDs was carried out mainly by the following three steps (as shown in Scheme 1): first, MnS cores were grown using thiol as a capping ligand; then the zinc precursor of various concentrations was injected into the solution for the growth of a ZnS buffer shell around the MnS core; subsequently, a CdS shell was grown by introducing the stock solution of cadmium precursor, leading to the formation of the MnS/ZnS/CdS core/shell QDs. Here, it should be pointed out that some of the Mn^{2+} ions in the MnS/ZnS QDs would diffuse from the MnS cores to the ZnS buffer layers,[32] and zinc and cadmium ions might mutually diffuse into their interface resulting in the formation of a $Cd_xZn_{1-x}S$ alloy layer during the synthesis process once the temperature was over 220 °C.

A representative synthesis procedure for the QDs is described as follows: 0.03 g of $MnSt_2$ and 12 mL of ODE were transferred into a 100 mL three necked flask and degassed for 20 min by bubbling Ar at 100 °C followed by heating up to 260 °C. Then the S stock solution was injected rapidly into the flask to form MnS nanoclusters (referred to as Sample A) and the color of the solution turned faint yellow. Subsequently, $ZnSt_2$ (0.06 g) solution was added to the reaction at 260 °C followed by heating up to 280 °C and maintaining the temperature for 10 min to coat the nanoclusters with ZnS (referred to Sample B), which allowed the growth of the ZnS buffer layer around the

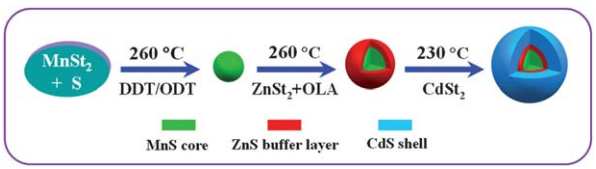

Scheme 1 Schematic illustration for the growth of MnS/ZnS/CdS QDs.

MnS core and favored the diffusion of the Mn^{2+} ions. Then the stock solution of cadmium precursor (7 mL) was added dropwise to the reaction flask at 230 °C in 1 mL, 2 mL, 2 mL, and 2 mL portions at intervals of 15 min to obtain QDs with different CdS shell thicknesses (referred to as Samples C, D, E, and F, respectively), followed by cooling to room temperature. The fabricated MnS/ZnS/CdS QDs were purified repeatedly using methanol/hexane and precipitated using acetone. Our experimental results suggest that the d-dots produced by the current procedure are highly reproducible.

2.5 Etching process

Etching experiments were carried out similar to Peng's work.[33] The OLA surface ligands of the QDs were exchanged for BLA to make the etching process more efficient. The BLA coated MnS/ZnS/CdS QDs were obtained by placing 0.5 mL of OLA coated NCs with a known size and concentration (*i.e.* 0.2 M) in ~2 mL of BLA, followed by sonication for ~15 min until the QDs were totally dispersed in a clear solution. The sonicated QD solution (0.5 mL) was then added to 2.5 mL of a chloroform–methanol solution (chloroform : methanol = 3 : 1). To initiate the etching process, each of the solutions was mixed with 0.5 mL of BPO (0.165 M) solution (chloroform : methanol = 1 : 1). The etching process was monitored using a Horiba Jobin Yvon Fluromax-4P spectrometer, which determined the PL measurements in real time with a good enough time resolution.

2.6 Structure and optical property characterization

UV-Vis measurements were carried out on a U-4100 UV-Vis-NIR scanning spectrophotometer. PL spectra, PL QY, and PL decays were recorded using a Horiba Jobin Yvon Fluromax-4P with a quantum-yield accessory and a time-correlated single-photon-counting (TCSPC) spectrometer. A pulsed xenon lamp was utilized as the excitation source for PL decay measurement. High-resolution transmission electron microscopy/transmission electron microscopy (HRTEM/TEM) images were recorded using a JEM-2100F electron microscope. The X-ray diffraction patterns of the fabricated samples were recorded on a Bruker D8 Advance powder diffractometer with Cu K_α (λ = 1.54 Å) as the incident radiation.

3 Results and discussion

3.1 Effect of CdS shell thickness on the structures and PL of MnS/ZnS/CdS QDs

Fig. 1 shows typical XRD patterns of the MnS core (Sample A), MnS/ZnS core/shell (Sample B), and MnS/ZnS/CdS core/shell QDs using the same amount of zinc precursor of 0.06 g and different amounts of cadmium precursor of 0.1 (Sample C), 0.3 (Sample D), and 0.5 g (Sample E). As shown in Fig. 1, the broad diffraction peaks with relatively low intensities typically characterize NCs. For the MnS cores, three peaks are located at 27.4°, 45.6°, and 54.0°, corresponding to diffractions from the (111), (220), and (311) planes, respectively, of zinc-blende phase MnS (JCPDS no. 40-1288). The diffraction pattern of the MnS/ZnS core/shell QDs is shifted towards a larger angle in comparison to that of the bare MnS cores. These peaks are consistent with the standard pattern of zinc-blende ZnS (JCPDS no. 05-0566).[32] For the MnS/ZnS/CdS core/shell QDs with different amounts of cadmium precursor, all three diffraction peaks are shifted to smaller angles as compared to those of the MnS/ZnS core/shell QDs. These peaks are located between the standard JCPDS no. 05-0566 (for cubic ZnS) and JCPDS no. 80-0019 (for cubic CdS), and become closer to JCPDS no. 80-0019 as the thickness of the CdS shell is increased, indicating that the MnS, ZnS, and CdS are all zinc-blende phases, and the lattice constant of the MnS (0.5614 nm) is between those of ZnS (0.5406 nm) and CdS (0.5811 nm). It is expected that the formation of the $Zn_xCd_{1-x}S$ alloy between the MnS core and the CdS shell with a suitable "*x*" value can adjust the average length of the cation–anion bond, which could match the optimal length of the Mn–S bond, benefiting Mn^{2+} ion diffusion and improving the PL properties.[8]

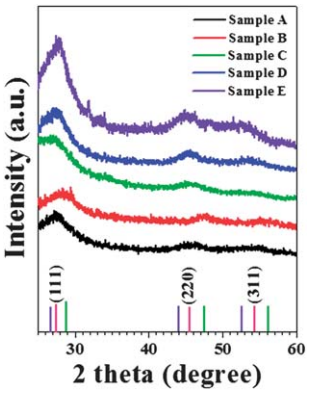

Fig. 1 Typical XRD patterns of the MnS core, MnS/ZnS, and MnS/ZnS/CdS NCs. The vertical pink, green, and violet bars show the standard diffraction patterns of zinc-blende bulk MnS (JCPDS no. 40-1288), ZnS (JCPDS no. 05-0566), and CdS (JCPDS no. 80-0019), respectively.

Fig. 2a and b show typical TEM images and the corresponding size distributions of the MnS/ZnS QDs produced using 0.06 g of $ZnSt_2$ (Sample B) and 0.06 g of $ZnSt_2$ + 0.5 g of $CdSt_2$ (Sample E), respectively. As depicted in Fig. 2, the QDs are nearly spherical and their sizes are ~2.8 and ~5.1 nm in Samples B and E, respectively. Based on the precursor mole ratio of $ZnSt_2$: $MnSt_2$ being 2 : 1 (similar to the ratio of Zn : Mn in the MnS/ZnS QDs detected by EDX (energy-dispersive X-ray

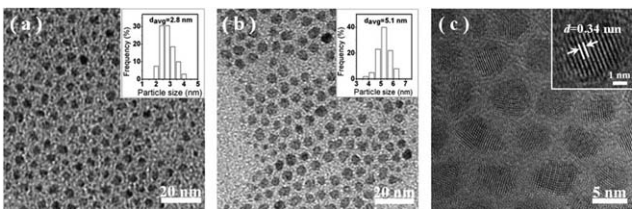

Fig. 2 (a) A typical TEM image and the size distribution (inset) of the MnS/ZnS QDs (Sample B). (b) A typical TEM image and the size distribution (inset) of the MnS/ZnS/CdS QDs (Sample E). (c) Typical HRTEM images of Sample E recorded under different magnifications.

spectroscopy) under TEM, the experimental setup is not shown here) for Sample B, the MnS core is ~2.1 nm (for the calculation of the ZnS/CdS layer thickness, see ESI†). Clear TEM images of the MnS cores are not provided here since it is difficult to obtain clean MnS QDs which are small, due to the large excess of ligands existing in the solution. Considering a thickness of 0.67 nm for 1 ML of the CdS shell in our case, the thickness of the CdS shell is estimated to be ~3.4 MLs, which is close to the theoretical thickness of 3.3 MLs (for the calculation of the ZnS/CdS layer thickness, see ESI†). Fig. 2c displays a representative HRTEM image of the MnS/ZnS/CdS QDs of Sample E. The inset shows a typical HRTEM image of a single QD with a diameter of 5.1 nm, suggesting the single-crystalline nature of the d-dots. It shows an interplanar spacing of 0.34 nm, corresponding to that of the (111) planes of zinc blend CdS (0.335 nm). For comparison, a typical HRTEM image of an MnS/ZnS QD is shown in the ESI (Fig. S1†). It is worth noting that no obvious crystal interface can be observed within the MnS/ZnS/CdS core/shell QDs or the MnS/ZnS core/shell QDs in the HRTEM images. This could be attributed to their similar lattice constants and mutual diffusion at their interfaces. The EDX results show that the average molar concentration of Mn^{2+} ions within Sample E is ~2.6%.

Fig. 3 shows typical absorption, PL, and PLE (photoluminescence excitation) spectra of Samples B, C, D, E, and F. The UV-Vis spectrum of the MnS/ZnS QDs is similar to that in our previous work.[9] As the amount of $CdSt_2$ precursor introduced is increased, the absorption peak of the MnS/ZnS/CdS QDs shifts obviously to a lower energy and reaches ~420 nm (Sample E), which is between the absorption band edges of the MnS/ZnS and MnS/CdS QDs with a size of ~5 nm (~450 nm as shown in Fig. 6a). This indicates that the CdS shell was successfully coated onto the MnS/ZnS QDs. The poorly resolved excitonic absorption peak might be characteristic of ternary and quaternary alloyed QDs, which are not caused solely by the wide size distribution, since the irregular composition distribution and the special electronic properties of the NCs are also considered as possible reasons.[34] The Mn^{2+} ion emission for Sample B is under the detectable level (Fig. 3), since the ZnS shell (~1 ML, for the calculation of the ZnS/CdS layer thickness, see ESI†) is too thin to limit the diffusion of the Mn^{2+} ions from the MnS core to the QD's surface.[32] However, it is interesting that, with the addition of cadmium precursor of up to 0.15 g (Sample C), a strong PL band can be observed at ~580 nm with a QY of 36%. This is clearly greater than that of the MnS/ZnS QDs with the same nominal amount of shell precursor, which may be due to the much lower reactivity of $ZnSt_2$ than that of $CdSt_2$. The peak energy (~2.14 eV) of the orange PL matches well the Mn ligand field transition energy ($^4T_1$ to $^6A_1$, ~2.12 eV), indicating that the PL originates from the typical emission of the Mn^{2+} ion due to its $^4T_1$ to $^6A_1$ transition (rather than the CdS band edge emission, since its absorption peak is at ~420 nm).[9,11,15,21,29] Furthermore, the PL of the CdS nanoparticles peaks at ~470 nm, which is distinctively different to that of the CdS:Mn QDs which is centered at around 580–590 nm, suggesting that the emission of the CdS:Mn QDs is from the Mn^{2+} ions rather than from the CdS shell (Fig. S2, ESI†). The PL QY first increases rapidly from 0 to an extremely high value of ~68% (the PL quantum yield (QY) measurements are shown in the ESI†) and then slightly decreases as the addition of cadmium precursor increases, indicating a significant improvement in the PL efficiency of the MnS/ZnS/CdS QDs due to a CdS passivating layer of a suitable thickness.[7] The excitation spectra of the orange emission by the MnS/ZnS/CdS core/shell QDs are consistent with the absorption onset, implying that the energy transfer is from the photoexcited MnS/ZnS/CdS shells to the Mn^{2+} ions. The onset in the excitation spectrum shifts to a lower energy with an increasing amount of cadmium precursor, suggesting an increase in the CdS shell thickness. However, the PL always peaks at ~580 nm as the CdS shell thickness is increased, which also confirms that the PL originates from the Mn ion emission, rather than the CdS band edge or trap state emission. This is because, in contrast to the excitons with size tunability *via* the quantum confinement effect, the energy of Mn luminescence is sensitive only to the changes in the local ligand field.[35]

Fig. 4 shows the PL decay curves of Mn^{2+} ions in the MnS/ZnS/CdS QDs with various CdS shell thicknesses. For these four samples, the emission detected at 580 nm exhibits a non-exponential decay, which can be fitted by a biexponential function:

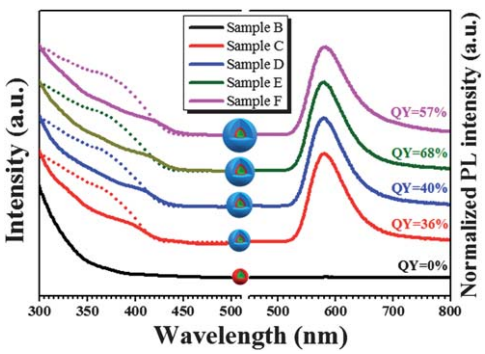

Fig. 3 The normalized UV-Vis absorption (left solid line), PLE (left dotted line), and PL (right) spectra of samples B (black lines), C (red lines), D (blue lines), E (green lines), and F (magenta lines), respectively.

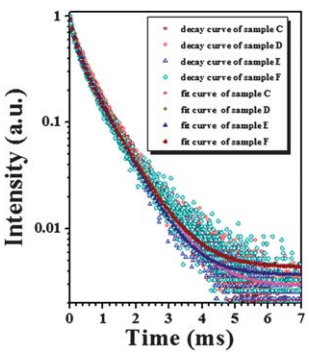

Fig. 4 The PL decay and corresponding fitting curves of MnS/ZnS/CdS QDs with various CdS shell thicknesses recorded at room temperature.

$$I(t) = y_0 + A_1\exp(-t/\tau_1) + A_2\exp(-t/\tau_2)$$

where τ_1 and τ_2 are the time constants, and A_1 and A_2 are the normalized amplitudes of the components.[9] The decay time constants of the two components are ~700 and ~180 μs, respectively (the PL decay and data fitting of the MnS/ZnS/CdS QDs are shown in the ESI†). To clarify the origin of the fast and slow decay components, the intensity ratio of the fast decay component (A_2t_2) to the slow one (A_1t_1) is described in Table 1. This shows that there is a positive correlation between the CdS shell thickness and the PL component with the fast decay. Therefore, the fast decay component cannot be explained by the radiative process of isolated Mn^{2+} ions, owing to the fact that the Mn^{2+} ions will be too far away from the surfaces of the QDs to decrease the nonradiative process as the shell thickness is increased.[6,9]

One may argue that the fast decay component might be attributed to the emission of the exciton or trap states which extend into the Mn^{2+} ion emission range. However, the lifetimes of exciton recombination and trap emission are in the range of 10^{-9} s and 10^{-10} s, respectively, so obviously cannot be as long as hundreds of μs.[36,37] It is known that the PL lifetime of Mn^{2+} pairs is shorter than that of a single Mn ion,[28] since the spin selection rule is relaxed and the electric dipole transition is allowed in the exchange coupled Mn^{2+} pairs. Thus, it can be deduced that the faster decay component with a time constant of 180 μs should be related to the exchange coupled Mn^{2+} ion pairs,[28,38] and the slower decay component should be attributed to the emission of the single isolated Mn^{2+} ions in cubic sites. On the other hand, the high intensity ratio of the fast decay component to the slow one implies a high dopant concentration of Mn^{2+} ions within the QDs, which could be tailored by optimizing the composition of the host. The positive correlation between the CdS shell thickness and the fast decay PL component can be attributed to the further diffusion of Mn^{2+} ions during the CdS shell growth. These results mean that our synthesized Mn:CdS d-dots only exhibit well-resolved Mn^{2+} ion emission with an extremely high QY, and the CdS band edge and surface defect or trap state emissions are suppressed, which is much superior to any Mn^{2+} ion doped cadmium based II–VI semiconductor QDs reported previously (Table S1, ESI†). This also allows us to explore the Mn^{2+} ion emission line shape without an overlapping contribution from surface states, and thus can be helpful for the deep investigation of the PL properties of Mn^{2+} ion doped cadmium based II–VI semiconductor QDs.

Table 1 Time constants τ_1 and τ_2, the corresponding amplitudes of the components A_1 and A_2, and the intensity ratios of the fast decay component to the slow decay component (A_2t_2/A_1t_1) of the MnS/ZnS/CdS QDs for samples C, D, E, and F

Sample	QY (%)	A_1	t_1 (μs)	A_2	t_2 (μs)	A_2t_2/A_1t_1
C	36	0.655	758.7	0.345	184.3	0.128
D	40	0.651	737.9	0.349	180.1	0.130
E	68	0.643	705.5	0.357	159.3	0.176
F	57	0.524	777.2	0.476	185.4	0.218

3.2 Effect of ligand on the growth of MnS/ZnS/CdS QDs

Control of the size of the MnSe (or MnS) core is considered an important issue for obtaining Mn^{2+} ion doped ZnSe (or ZnS) d-dots of high quality *via* the nucleation-doping strategy. It has been reported that small MnSe cores of high stability could be obtained at a growth temperature of 260 °C when the ratio of Se to Mn precursor was up to 25 : 1.[7] However, our previous work suggested that it was not suitable for the synthesis of small and stable MnS QDs to use a large excess of S precursor, even if the reaction was terminated just after the mixing of the Mn and S precursors at the high temperature.[32] In these experiments, alkyl amines such as octadecylamine (ODA)[9] and OLA[11] were used predominantly as the capping ligands for the growth of MnS and MnSe QDs. The choice of the capping ligand is a key issue for the controlled growth of NCs, because an appropriate ligand can limit the growth of NCs remarkably to form small NCs of high quality.[39] Here, noting that the coordination and binding ability of the mercapto group are stronger than those of phosphorous, oxygenous, and nitrogenous groups,[2,12] we selected the thiols such as 1-dodecanethiol (DDT) and 1-octadecanethiol (ODT) as the capping ligands to obtain stable and small MnS cores. Fig. 5a shows the absorption spectra of the corresponding MnS NCs with the ligands OLA, ODT, and DDT. The absorption onsets suggest an obvious blue-shift when the thiols are used as the capping ligands to replace ODA, which is consistent with the theory. The absorption onset of the MnS NCs with the DDT ligand is blue shifted compared to that with the ODT ligand, which can be attributed to the fact that the size of the NCs is strongly dependent on the boiling point of the ligand.[40] In our case, the growth temperature for the MnS cores was 260 °C, which is higher than the boiling point of ODT (204–210 °C) and lower than that of DDT (266–283 °C). As shown in Fig. 5b, with the same thicknesses of the ZnS buffer layer and the CdS shell, 1 ML and 3.3 MLs, respectively, the PL QYs of the corresponding MnS/ZnS/CdS NCs are 28%, 43%, and 68% when OLA, ODT, and DDT are used as the ligands, respectively. During the preparation of this article, we noticed that Zhong's group[12] has used DDT to synthesize Mn^{2+} ion doped ZnS d-dots with a high PL QY, also suggesting the advantages of thiol ligands for obtaining stable and small MnS cores. We optimized

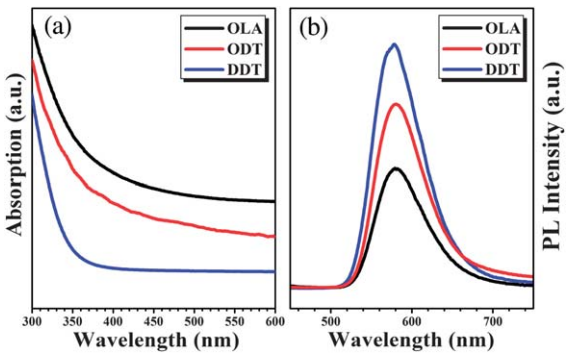

Fig. 5 (a) UV-Vis absorption spectra of the MnS cores and (b) PL spectra of the MnS/ZnS/CdS QDs with OLA (black lines), ODT (red lines), and DDT (blue lines) as the capping ligand of the MnS cores.

the amount of thiol to 0.2 mL and added enough ODE–S and alkyl amine, which favored the successful fabrication of highly efficient MnS/ZnS/CdS NCs with good reproducibility. Moreover, it is promising that this synthetic strategy could also be applied for the fabrication of other Mn^{2+} ion doped II–VI semiconductor NC hosts, such as Mn:CdSe and Mn:ZnSe.

3.3 Effect of ZnS buffer layer thickness on the PL properties of MnS/ZnS/CdS QDs

In our synthesis strategy, control of the thickness of the ZnS buffer layer within the MnS/ZnS/CdS NCs was accomplished by tailoring the amount of the introduced zinc precursor during the growth of the QDs. The amount of zinc precursor was adjusted from 0 to 0.63 mmol (0 to 0.4 g) with a constant total amount of Cd and Zn precursor of 0.84 mmol to retain a nominally fixed particle size, which led to the formation of the ZnS layer with a tailored thickness (for the calculation of the ZnS/CdS layer thickness, see ESI†). Fig. 6 shows the UV-Vis absorption and PL spectra of the MnS/ZnS/CdS QDs with various ZnS buffer layer thicknesses. It seems that there is a systematic variation in the absorption peak position (Fig. 6a). The QDs without the ZnS buffer layer show an absorption band edge of CdS at ~450 nm. The absorption band edge shows a blue shift and gradually tends towards the absorption band edge of ZnS as the ZnS buffer layer thickness is increased, providing powerful evidence for the successful coating of the ZnS buffer layer around the MnS core. Fig. 6b shows representative PL spectra of the MnS/ZnS/CdS QDs with various thicknesses of ZnS buffer layer. The PL spectrum of Sample A without the ZnS buffer layer is distinctively different from the others, and exhibits broad PL with a full width at half-maximum (FWHM) of ~300 nm (Fig. 6b) and a low PL QY of 8% (Fig. 6c). However, after the ZnS buffer layer is introduced, even when the CdS shell is no more than 1 ML thick, the doped NCs exhibit well-resolved Mn^{2+} ion emission and the CdS band edge and surface state emissions are suppressed to an undetectable level. This indicates that the ZnS buffer layer makes a significant contribution to the growth of highly luminescent Mn:CdS QDs. The PL QY of the Mn^{2+} ions increases with increasing ZnS layer thickness at first, and reaches a maximum (68%) at a thickness of 1 ML, then decreases as the ZnS layer thickness is further increased (Fig. 6c). Klimov predicted that Mn^{2+} ion doping of $Cd_{1-x}Zn_xS$ alloys should be most favorable at an alloy composition of approximately $x = 0.5$, because, at this composition, the excess enthalpy of Mn^{2+} ion doping is minimized.[41] Herein, it is anticipated that the thickness-dependent Mn^{2+} ion emission could be caused by different values of "x" in the $Zn_xCd_{1-x}S$ alloy at the interface between the ZnS buffer layer and the CdS shell, since a different ZnS buffer layer will result in the formation of $Zn_xCd_{1-x}S$ alloy layers with various values of "x".[8,29] However, despite the change expected in the PL QY (Fig. 6c), the normalized PL spectra of the above four samples show almost the same spectral contours (Fig. 6b) and peak positions (centered at ~580 nm) when the buffer layer thickness is changed from 0.6 to 3.6 MLs (Fig. 6c). It should be pointed out that, contrary to the reported PL of MnS/ZnS QDs[32] (peak at ~590 nm), the ZnS buffer layer may be thick enough (*i.e.* in Sample F) to prevent the diffusion of Mn^{2+} ions into the CdS shell,[32] and the PL of the MnS/ZnS/CdS QDs also shows a blue-shift relative to that of the MnS/ZnS NCs, which seems contrary to the theoretical predictions. To understand this blue-shift, we monitored the reaction process of the second step involving the addition of 0.4 g of zinc precursor (equivalent to a 3.6 ML ZnS layer) and the third step involving the growth of the CdS passivating layer, which is recorded in Fig. 7a. This suggests that the PL of the MnS/ZnS QDs with a 3.6 ML ZnS shell (black line) is centered at ~590 nm. However, after a CdS shell layer is grown, regardless of the thickness, Mn^{2+} ion emission shifts rapidly to ~580 nm. That is to say, the blue-shift occurs during the process of CdS shell coating.

Now we come to discuss what causes the blue-shift. One point of view is that the fast blue-shift of the PL peak position after the CdS shell coating can be ascribed to the presence of residual Mn^{2+} ions, which could not be consumed completely during the growth of the MnS cores and ZnS buffer layer. The

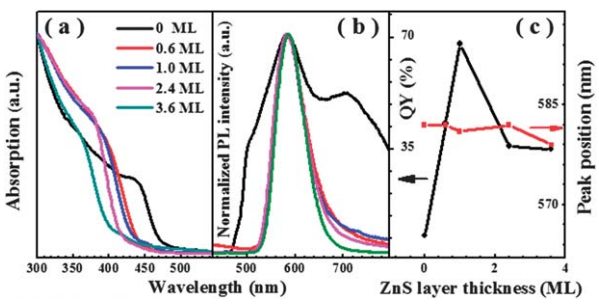

Fig. 6 (a) Representative UV-Vis absorption and (b) PL spectra of MnS/ZnS/CdS QDs with various thicknesses of the ZnS layer. The excitation wavelength was 365 nm. (c) The PL QYs and peak positions of the MnS/ZnS/CdS QDs as a function of the ZnS layer thickness.

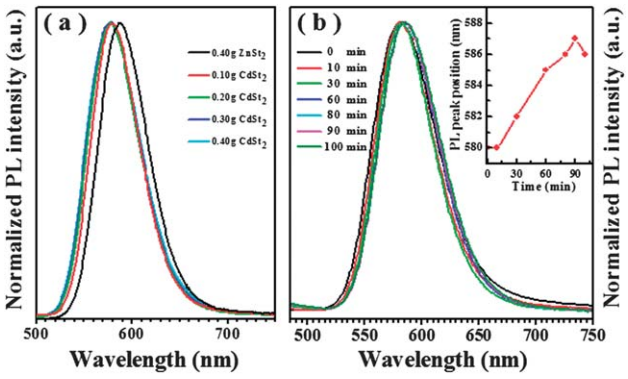

Fig. 7 (a) PL spectra of MnS/ZnS and MnS/ZnS/CdS QDs synthesized using different amounts of zinc and cadmium precursors. The amount of zinc precursor was 0.4 g of $ZnSt_2$ (black line) for the preparation of MnS/ZnS NCs, and a further 0.1 g of $CdSt_2$ (green line), 0.2 g of $CdSt_2$ (blue line), 0.3 g of $CdSt_2$ (cyan line), and 0.4 g of $CdSt_2$ (magenta line) were used for the preparation of the MnS/ZnS/CdS QDs. The MnS/ZnS/CdS and MnS/ZnS QD NCs were excited at 365 and 265 nm, respectively. (b) The temporal evolution of the PL spectra of the MnS/ZnS/CdS QDs with a thick ZnS buffer layer of 3.6 MLs etched using BOP. The inset shows the PL peak position of the QDs as a function of the etching time.

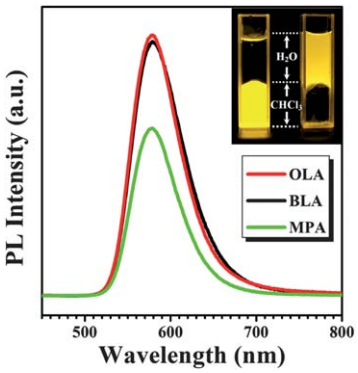

Fig. 8 Typical PL spectra of MnS/ZnS/CdS QDs before and after ligand exchange. The QDs are coated with a layer of OLA (red line), BLA (black line) or MPA (green line). The inset shows the digital photographs of the MnS/ZnS/CdS QDs dissolved in $CHCl_3$ (left) and water (right) excited at 365 nm.

residual Mn^{2+} ions could be doped into the CdS shell during the growth of the QDs in the third step. However, our experiments exclude the above hypothesis. For small MnS cores, we first used 0.4 g of zinc precursor to form a ZnS shell layer. Then the synthesis was terminated suddenly by cooling the reaction solution to room temperature rapidly. The obtained QDs were purified in a standard way to clean them of residual chemical reagent, and then dissolved in a mixture solution of ODE and OLA. The resulting solution was heated at a much lower coating temperature of 220 °C to hinder the decomposition of the MnS/ZnS QDs caused by Ostwald ripening,[32] and the MnS/ZnS QDs were further coated with a CdS shell, resulting in the growth of MnS/ZnS/CdS QDs. We recorded the PL evolution of these separate samples (Fig. S3, ESI†) and found that the shift of the PL peak was very similar to that in Fig. 7b. Thus, it is strongly suggested that the fast blue-shift of the PL peak position cannot be attributed to the doping of the residual Mn^{2+} ions into the CdS shell or the diffusion of the Mn^{2+} ions into the CdS shell because of the low coating temperature of 220 °C and the thick ZnS buffer layer.[32] Another explanation for the blue-shift might be that it is due to cation exchange between Cd and Zn chalcogenides occurring in preference to CdS shell growth. It is well known that cation exchange between Cd and Zn chalcogenide is kinetically favored and it is feasible to generate composition controlled $Cd_xZn_{1-x}Se$ alloyed NCs.[42,43] So one may argue that the blue-shift of the PL might come from the partial or total replacement of ZnS with a CdS component, since the peak position of the Mn^{2+} ion emission in ZnS QDs is 590 nm while it is bluer (~580 nm) in CdS. However, it is difficult for the cation exchange reaction to occur due to the large excess of the S precursor in our case.[43] Also, our following etching experiments exclude the above hypothesis. Fig. 7b shows the evolution of the PL peak position of the MnS/ZnS/CdS QDs with a thick ZnS buffer layer of 3.6 MLs during the etching process. Before the addition of BPO, the fluorescence peak of the QDs is centered at ~580 nm. However, the PL peak position shifts to 587 nm as the etching time is changed within 90 min. In other words, with the removal of the outer shell, the fluorescence peak position of the QDs reverts to that of those without the CdS shell. In principle, if the blue-shift is caused by the host of the d-dots changing from ZnS to the $Cd_xZn_{1-x}S$ alloy, the shift of the PL should not happen during the etching process, which is in contrast to the experimental results. Here, we explain the blue-shift by the ligand field theory, which has successfully described the electronic structures of Mn^{2+} ions in a wide variety of coordination environments. The lattice constant of CdS (0.581 nm) is larger than that of ZnS (0.541 nm), which could result in tensile stress once a CdS shell layer is coated on the MnS/ZnS QDs. When the crystal field of the Mn^{2+} ion is formed under a certain force, the transition energy gap of the Mn^{2+} ion emission could be increased, and in turn, might lead to the blue-shift of the PL peak position.

Fig. 8 shows the PL spectra of the MnS/ZnS/CdS QDs (Sample E) before and after ligand exchange. It seems that these hydrophobic MnS/ZnS/CdS QDs could be made water-soluble by coating with a layer of MPA through ligand exchange. The water-soluble QDs show excellent stability for at least 3 months with a PL QY of up to 46%, which suggests the potential and advantage of our fabricated QDs for utilization in biomedical applications. In addition, it is well known that the performance of hybrid organic/inorganic LEDs with colloidal QDs as emission centers will be significantly influenced by surface ligands. The QDs passivated with shorter ligands will favor much better charge injection and energy transfer, as well as an improved quality of the hybrid film.[44] The carbon chain length of BLA is much shorter than that of OLA. It is interesting to find that the PL QY of MnS/ZnS/CdS QDs coated with BLA *via* ligand exchange reaches up to 66% (Fig. 8, black line), which is almost the same as that of the QDs coated with OLA. That is to say, the fabricated MnS/ZnS/CdS QDs cannot only be made water-soluble, but can also be coated by ligands with short carbon chain lengths nearly without cost to the PL QY, which could strongly recommend our MnS/ZnS/CdS QDs for practical applications in biology/biomedicine and opto/electronic devices.

4 Conclusions

In summary, we have reported a strategy for the controlled growth of MnS/ZnS/CdS QDs (Mn:CdS QDs), which were synthesized by using a thiol as the capping ligand rather than the conventional alkyl amines for the growth of small MnS cores of high quality, combined with a ZnS buffer layer introduced before the growth of the CdS shell. The experimental results suggest that the designed interface buffer layer of ZnS plays a critical role in the improvement of the PL properties of the fabricated Mn:CdS QDs. The as-synthesized QDs possess an extremely high PL QY of up to 68%, which is more than two times that of the highest QY of Mn^{2+} ion doped cadmium based II–VI semiconductor QDs previously reported. These d-dots exhibit well-resolved Mn^{2+} ion emission, without any CdS band edge and surface state emission. Moreover, our MnS/ZnS/CdS QDs cannot only be made water-soluble, but can also be coated by ligands with short carbon chains nearly without cost to the PL QY. The current work could strongly recommend the Mn:CdS d-dots for practical applications in biology/biomedicine and opto/electronic devices.

Acknowledgements

This work was supported by the National Natural Science Foundation of China (NSFC, grant no. 61106066, 21101038, and 60976049), 973 program (grant no. 2012CB326407), Zhejiang Provincial Science Foundation for Distinguished Young Scholars (grant no. R4100242), Zhejiang Provincial Nature Science Foundation (grant no. Y4110529), Ningbo Municipal Natural Science Foundation (grant no. 2011A610093 and 2011A610094). J. L. Zhao thanks the support of the Hundred Talent Program of the Chinese Academy of Sciences.

Notes and references

1 A. Nag and D. Sarma, *J. Phys. Chem. C*, 2007, **111**, 13641.
2 N. Pradhan, D. M. Battaglia, Y. Liu and X. Peng, *Nano Lett.*, 2007, **7**, 312.
3 R. Beaulac, L. Schneider, P. I. Archer, G. Bacher and D. R. Gamelin, *Science*, 2009, **325**, 973.
4 S. C. Erwin, L. Zu, M. I. Haftel, A. L. Efros, T. A. Kennedy and D. J. Norris, *Nature*, 2005, **436**, 91.
5 Y. Yang, O. Chen, A. Angerhofer and Y. C. Cao, *J. Am. Chem. Soc.*, 2006, **128**, 12428.
6 A. Nag, S. Sapra, C. Nagamani, A. Sharma, N. Pradhan, S. Bhat and D. Sarma, *Chem. Mater.*, 2007, **19**, 3252.
7 N. Pradhan and X. Peng, *J. Am. Chem. Soc.*, 2007, **129**, 3339.
8 A. Nag, S. Chakraborty and D. Sarma, *J. Am. Chem. Soc.*, 2008, **130**, 10605.
9 J. Zheng, X. Yuan, M. Ikezawa, P. Jing, X. Liu, Z. Zheng, X. Kong, J. Zhao and Y. Masumoto, *J. Phys. Chem. C*, 2009, **113**, 16969.
10 S. Acharya, D. D. Sarma, N. R. Jana and N. Pradhan, *J. Phys. Chem. Lett.*, 2010, **1**, 485.
11 R. Zeng, T. Zhang, G. Dai and B. Zou, *J. Phys. Chem. C*, 2011, **115**, 3005.
12 W. Zhang, Y. Li, H. Zhang, X. Zhou and X. Zhong, *Inorg. Chem.*, 2011, **50**, 10432.
13 R. Bhargava, D. Gallagher, X. Hong and A. Nurmikko, *Phys. Rev. Lett.*, 1994, **72**, 416.
14 Z. Quan, D. Yang, C. Li, D. Kong, P. Yang, Z. Cheng and J. Lin, *Langmuir*, 2009, **25**, 10259.
15 B. B. Srivastava, S. Jana, N. S. Karan, S. Paria, N. R. Jana, D. D. Sarma and N. Pradhan, *J. Phys. Chem. Lett.*, 2010, **1**, 1454.
16 J. Zhuang, X. Zhang, G. Wang, D. Li, W. Yang and T. Li, *J. Mater. Chem.*, 2003, **13**, 1853.
17 W. Chen, V. F. Aguekian, N. Vassiliev, A. Y. Serov and N. G. Filosofov, *J. Chem. Phys.*, 2005, **123**, 124707.
18 A. A. Bol and A. Meijerink, *Phys. Rev. B: Condens. Matter Mater. Phys.*, 1998, **58**, R15997.
19 A. Nag, R. Cherian, P. Mahadevan, A. V. Gopal, A. Hazarika, A. Mohan, A. Vengurlekar and D. Sarma, *J. Phys. Chem. C*, 2010, **114**, 18323.
20 Y. Yang, O. Chen, A. Angerhofer and Y. C. Cao, *J. Am. Chem. Soc.*, 2008, **130**, 15649.
21 Y. Yang, O. Chen, A. Angerhofer and Y. C. Cao, *Chem.–Eur. J.*, 2009, **15**, 3186.
22 R. Zeng, M. Rutherford, R. Xie, B. Zou and X. Peng, *Chem. Mater.*, 2010, **22**, 2107.
23 R. Beaulac, P. I. Archer, X. Liu, S. Lee, G. M. Salley, M. Dobrowolska, J. K. Furdyna and D. R. Gamelin, *Nano Lett.*, 2008, **8**, 1197.
24 R. Beaulac, P. I. Archer, J. van Rijssel, A. Meijerink and D. R. Gamelin, *Nano Lett.*, 2008, **8**, 2949.
25 F. V. Mikulec, M. Kuno, M. Bennati, D. A. Hall, R. G. Griffin and M. G. Bawendi, *J. Am. Chem. Soc.*, 2000, **122**, 2532.
26 G. M. Dalpian and J. R. Chelikowsky, *Phys. Rev. Lett.*, 2006, **96**, 226802.
27 A. Ishizumi and Y. Kanemitsu, *Adv. Mater.*, 2006, **18**, 1083.
28 A. Ishizumi, E. Jojima, A. Yamamoto and Y. Kanemitsu, *J. Phys. Soc. Jpn.*, 2008, **77**, 053705.
29 W. Xu, X. Meng, W. Ji, P. Jing, J. Zheng, X. Liu, J. Zhao and H. Li, *Chem. Phys. Lett.*, 2012, **532**, 72.
30 R. Shannon, *Acta Crystallogr., Sect. A: Cryst. Phys., Diffr., Theor. Gen. Crystallogr.*, 1976, **32**, 751.
31 T. Zuo, Z. Sun, Y. Zhao, X. Jiang and X. Gao, *J. Am. Chem. Soc.*, 2010, **132**, 6618.
32 J. Zheng, W. Ji, X. Wang, M. Ikezawa, P. Jing, X. Liu, H. Li, J. Zhao and Y. Masumoto, *J. Phys. Chem. C*, 2010, **114**, 15331.
33 D. Battaglia, B. Blackman and X. Peng, *J. Am. Chem. Soc.*, 2005, **127**, 10889.
34 N. C. Greenham, X. Peng and A. P. Alivisatos, *Phys. Rev. B: Condens. Matter Mater. Phys.*, 1996, **54**, 17628.
35 R. Beaulac, P. I. Archer, S. T. Ochsenbein and D. R. Gamelin, *Adv. Funct. Mater.*, 2008, **18**, 3873.
36 S. Sapra, A. Prakash, A. Ghangrekar, N. Periasamy and D. Sarma, *J. Phys. Chem. B*, 2005, **109**, 1663.
37 J. Zhang, X. Zhang and J. Zhang, *J. Phys. Chem. C*, 2009, **113**, 9512.
38 L. Qian, D. Bera and P. Holloway, *Appl. Phys. Lett.*, 2008, **92**, 093103.
39 N. I. Hammer, T. Emrick and M. D. Barnes, *Nanoscale Res. Lett.*, 2007, **2**, 282.
40 N. Pradhan, D. Reifsnyder, R. Xie, J. Aldana and X. Peng, *J. Am. Chem. Soc.*, 2007, **129**, 9500.
41 V. I. Klimov, *Nanocrystal quantum dots*, CRC Press, Boca Raton, FL, 2010.
42 X. Zhong, Y. Feng, Y. Zhang, Z. Gu and L. Zou, *Nanotechnology*, 2007, **18**, 385606.
43 S. Acharya and N. Pradhan, *J. Phys. Chem. C*, 2011, **115**, 19513.
44 A. M. Munro, J. A. Bardecker, M. S. Liu, Y. J. Cheng, Y. H. Niu, I. J. L. Plante, A. K. Y. Jen and D. S. Ginger, *Microchim. Acta*, 2008, **160**, 345.